Hindawi Publishing Corporation
Mathematical Problems in Engineering
Volume 2012, Article ID 802414, 22 pages
doi:10.1155/2012/802414

Research Article

A Meshless Finite-Point Approximation for Solving the RLW Equation

L. Pérez Pozo,[1] R. Meneses,[2] C. Spa,[2] and O. Durán[3]

[1] *Aula UTFSM-CIMNE, Departamento de Ingeniería Mecánica, Universidad Técnica Federico Santa María, Avenida España 1680, 2340000 Valparaíso, Chile*
[2] *Departamento de Matemática, Universidad Técnica Federico Santa María, Avenida España 1680, 2340000 Valparaíso, Chile*
[3] *Escuela de Ingeniería Mecánica, Pontificia Universidad Católica de Valparaíso, Los Carrera 01567, Quilpué, 2430120 Valparaíso, Chile*

Correspondence should be addressed to L. Pérez Pozo, luis.perez@usm.cl

Received 20 October 2011; Revised 5 January 2012; Accepted 15 January 2012

Academic Editor: Gradimir V. Milovanović

Copyright © 2012 L. Pérez Pozo et al. This is an open access article distributed under the Creative Commons Attribution License, which permits unrestricted use, distribution, and reproduction in any medium, provided the original work is properly cited.

An alternative meshless finite-point method (FPM) technique for the numerical solution of the Regularized long wave (RLW) equation is presented. In this context, we derive the discretized system by combining finite difference (FD) techniques for the time derivative and FPM for the spatial derivatives. The accuracy of this alternative approach is tested with L_2, L_∞ error norms and the conservation properties of mass, energy, and momentum under the RLW equation.

1. Introduction

The numerical analysis of nonlinear dispersive waves has significant importance in physical phenomena, such as shallow water waves [1], ion acoustic solitary waves [2], motion for mixtures of liquid and gas bubbles [3], and so on. Importantly, the regularized long wave (RLW) equation is an alternative description to the well-known Korteweg-de Vries (KdV) equation [4]. Like the KdV equation, the RLW equation also describes a large number of physical phenomena; see [5, 6]. The first formulation of the RLW equation was presented by Peregrine [7] to describe the behavior of an undular bore with a numerical solution based on a finite difference (FD) method with first-order accuracy in terms of time. In the recent years, several numerical methods for the solution of the RLW equation have been developed, including FD methods [8–11], Fourier pseudospectral (PS) methods [12], finite element methods (FEMs) based on Galerkin and collocation techniques [13–19]. Furthermore, focusing on a meshless context, Shokri and Dehghan [20] presented an approach for solving the RLW equation with radial basis functions (RBFs) by using FD to yield the time derivative

as well as a predictor-corrector procedure to solve the nonlinear system. In addition, Islam et al. [21] also applied RBF and FD to the time derivative, but they addressed nonlinear behavior with the θ-weighted scheme. These recent works and references mentioned therein present helpful reviews on the RLW equation and related aspects.

Meshless methods are a family of numerical techniques that do not require a *mesh*. In these methods, the body or domain is discretized by a collection of points. It is divided into local interpolation subdomains, which are also called *clouds*; they consist of one central point, or *star node*, and several neighboring points. Generally, these methods are computationally efficient and easy to implement, and they have been successfully used in several application. The general characteristics, classifications, advantages, and disadvantages of these methods can be found in [22–26]. *Meshless* finite point method (FPM) approximation around each point is obtained using weighted least square techniques. The discrete system of equation is constructed based on a point collocation procedure. This method was proposed in [27, 28] to solve convective transport and fluid flow problems. Its application has been extended to advection-diffusion transport [29], incompressible flow problems [30], elasticity [31, 32], solid dynamics [33], solidification modeling [34], nonlinear material behavior problems [35, 36], adaptive refinement [37, 38], and large deflection analysis of flexible plates [39]. The lack of dependence on a mesh or integration procedure is an important feature, making the FPM a truly meshless method. This work is structured as follows. In Section 2, the FPM is introduced. The meshless FPM implementation of the RLW equation is developed in Section 3. In Section 4, the accuracy of this approach is tested with respect to L_2, L_∞ error norms and the conservation properties of mass, energy and momentum [40]. The numerical simulation includes the propagation of a solitary wave, the interaction of two positive solitary waves, the interaction of a positive and a negative solitary wave, the evaluation of *Maxwellian* pulse into stable solitary waves, and the development of an undular bore. Finally, conclusions to the current investigation are shown in Section 5.

2. The Finite Point Method

Although the FPM introduced by Oñate et al. was originally formulated for the numerical solution of convective transport and fluid flow problems, it can be easily adapted to the RLW equation. In this section, we review the basic formulation of the FPM and provide a brief overview of its main features. In order to obtain the final system of discrete equations, the FPM approximates the local solution of a partial differential equation in each point of the discretized domain by means of a weighted least squares technique and a point collocation procedure. Due to the local character of the approximation procedure used by this method, it is necessary to define a subdomain Ω_k for each node x_k. This Ω_k contain neighboring nodes selected by a suitable criterion [31, 41, 42]. This collection of nodes is called a *cloud*, and its referential central point is the *star node*. For example, a relevant aspect in the definition of *clouds* is that their superposition must produce the whole domain, Ω:

$$\Omega \subseteq \bigcup_{k=1}^{N_p} \Omega_k, \tag{2.1}$$

where N_p is the total number of nodes. Note that the definition of *clouds* is the basic, initial step in implementing the FPM approximation using fixed weighted least squares. With the

discretized domain defined, let us define a function $u(x)$, which is locally approximated by $\widehat{u}(x)$ only valid in the subdomain Ω_k associated with the *star node* x_k as a linear combination of known functions $\mathbf{p}(x)$:

$$u(x) \cong \widehat{u}(x) = \mathbf{p}(x)\boldsymbol{\alpha}_{\mathbf{k}} \quad \forall x \in \Omega_k, \tag{2.2}$$

where $\mathbf{p}(x)$ is the vector that represents the basis of m linearly independent functions and $\boldsymbol{\alpha}_{\mathbf{k}}$ is a vector of constant parameters only valid in Ω_k. The elements of the interpolation base may belong to any function family. In this paper the m first monomial polynomials are used; that is, $\mathbf{p}(x) = [1 \; x \; x^2 \cdots \; x^{m-1}]$. Since (2.2) is valid for all N_c points of the kth subdomain, the approximations $\widehat{u}(\mathbf{X})$ conform to a *Vandermonde* system given by the following relation:

$$\mathbf{u}\left(\mathbf{X}^{\mathbf{k}}\right) \cong \widehat{\mathbf{u}}\left(\mathbf{X}^{\mathbf{k}}\right) = \mathbf{P}\left(\mathbf{X}^{\mathbf{k}}\right) \cdot \boldsymbol{\alpha}_{\mathbf{k}}, \tag{2.3}$$

where

$$\begin{gathered}
\mathbf{X}^{\mathbf{k}} = [x_{k,1} \cdots x_{k,N_c}]^T, \qquad \mathbf{u}\left(\mathbf{X}^{\mathbf{k}}\right) = [u(x_{k,1}) \cdots u(x_{k,N_c})]^T, \\
\widehat{\mathbf{u}}\left(\mathbf{X}^{\mathbf{k}}\right) = [\widehat{u}(x_{k,1}) \cdots \widehat{u}(x_{k,N_c})]^T, \qquad \boldsymbol{\alpha}_{\mathbf{k}} = [\alpha_{k,1} \cdots \alpha_{k,N_c}]^T, \\
\mathbf{P}\left(\mathbf{X}^{\mathbf{k}}\right) = \begin{bmatrix} \mathbf{p}(x_{k,1}) \\ \vdots \\ \mathbf{p}(x_{k,N_c}) \end{bmatrix}.
\end{gathered} \tag{2.4}$$

In general, the number of points N_c that conform to the *cloud* is greater than the number of functions m that define the basis; hence, the matrix $\mathbf{P}(\mathbf{X}^{\mathbf{k}})$ is usually rectangular. This means that the property of interpolation is lost, and the problem must be addressed with numerical approximation. The coefficients of the vector $\boldsymbol{\alpha}_{\mathbf{k}}$ must be determined in such a way that the weighted sums of the squared differences between the exact values $u(x)$ and the approximated values $\widehat{u}(x)$ of each point are minimized according to the following expression:

$$\min\left\{\sum_{j=1}^{N_c} w(x_{k,j}) \cdot \left(u(x_{k,j}) - \widehat{u}(x_{k,j})\right)^2\right\}, \tag{2.5}$$

where $w(x)$ is a fixed weighting function defined in Ω_k. See [27, 28]. The minimization process described by (2.5) leads to the following expression for vector $\boldsymbol{\alpha}_{\mathbf{k}}$:

$$\boldsymbol{\alpha}_{\mathbf{k}} = \mathbf{A}^{-1}\left(\mathbf{X}^{\mathbf{k}}\right)\mathbf{B}\left(\mathbf{X}^{\mathbf{k}}\right)\boldsymbol{\lambda}\left(\mathbf{X}^{\mathbf{k}}\right), \tag{2.6}$$

where $\boldsymbol{\lambda}(\mathbf{X}^{\mathbf{k}})$ is a vector that represents the unknown parameters sought on the *cloud* Ω_k defined as follows:

$$\boldsymbol{\lambda}\left(\mathbf{X}^{\mathbf{k}}\right) = [\lambda(x_{k,1}) \cdots \lambda(x_{k,N_c})]^T. \tag{2.7}$$

Additionally, matrices $\mathbf{A}(\mathbf{X}^{\mathbf{k}})$, $\mathbf{B}(\mathbf{X}^{\mathbf{k}})$, and $\mathbf{W}(\mathbf{X}^{\mathbf{k}})$ are given as follows:

$$\mathbf{A}\left(\mathbf{X}^{\mathbf{k}}\right) = \mathbf{P}\left(\mathbf{X}^{\mathbf{k}}\right)\mathbf{W}\left(\mathbf{X}^{\mathbf{k}}\right)\mathbf{P}^{T}\left(\mathbf{X}^{\mathbf{k}}\right), \qquad \mathbf{B}\left(\mathbf{X}^{\mathbf{k}}\right) = \mathbf{P}^{T}\left(\mathbf{X}^{\mathbf{k}}\right)\mathbf{W}\left(\mathbf{X}^{\mathbf{k}}\right), \tag{2.8}$$

and $\mathbf{W}(\mathbf{X}^{\mathbf{k}})$ is an $N_c \times N_c$ diagonal matrix defined by

$$\mathbf{W}\left(\mathbf{X}^{\mathbf{k}}\right) = \left[\operatorname{diag}(w(x_{k,1}) \cdots w(x_{k,N_c}))\right], \tag{2.9}$$

where the weighting functions $w(x)$ are derived in order to have unit values near the *star node* and zero values outside the Ω_k subdomains. Under the FPM, the common selection for the fixed weighting function is given as follows:

$$w(x) = \begin{cases} \dfrac{\exp\left(-(h_j/\zeta)^2\right) - \exp\left(-(r/\zeta)^2\right)}{1 - \exp\left(-(r/\zeta)^2\right)}, & \text{if } h_j \le r, \\ 0, & \text{if } h_j > r, \end{cases} \tag{2.10}$$

where h_j is the distance between the *star node* x_k and the point x, $r = q \cdot h_{\max}$ (max. of h_j) is a reference distance, and $\zeta = \beta \cdot r$. A detailed description of the effects of the constant parameters q and β on numerical approximation as well as guidelines for setting their values is presented in [43]. Other considerations in selecting the function $w(x)$ can be found in [27, 28, 44, 45]. Finally, replacing (2.6) in (2.2), the next relation is obtained:

$$\widehat{u}(x) = \mathbf{N}^{T}(x)\boldsymbol{\lambda}\left(\mathbf{X}^{\mathbf{k}}\right), \tag{2.11}$$

where $\mathbf{N}(x)$ is a matrix called *shape function* defined by

$$\mathbf{N}(x) = \mathbf{p}^{T}(x)\mathbf{C}\left(\mathbf{X}^{\mathbf{k}}\right), \tag{2.12}$$

with $\mathbf{C}(\mathbf{X}^{\mathbf{k}}) = \mathbf{A}^{-1}(\mathbf{X}^{\mathbf{k}})\mathbf{B}(\mathbf{X}^{\mathbf{k}})$. We remark that $\mathbf{p}(x)$ denote $[1 \; x \; x^2 \cdots \; x^{m-1}]$. Note that according to the least square nature of the approximation, $u(x) \cong \widehat{u}(x) \neq \lambda(x)$; that is, the local values of the approximating function do not fit the nodal unknown values. Indeed, $\widehat{u}(x)$ is the true approximation, which we be will used to satisfy the differential equation and the boundary conditions; in this context, $\lambda(x)$ are simply the unknown parameters we aim to determine. According to the concepts described above and (2.11), it is possible to obtain the following expressions:

$$\widehat{u}_x(x) = \mathbf{N}_x^{T}(x)\boldsymbol{\lambda}\left(\mathbf{X}^{\mathbf{k}}\right) \qquad \widehat{u}_{xx}(x) = \mathbf{N}_{xx}^{T}(x)\boldsymbol{\lambda}\left(\mathbf{X}^{\mathbf{k}}\right), \tag{2.13}$$

where $(\cdot)_x$ and $(\cdot)_{xx}$ denote the first and the second space derivatives, respectively. Note that these derivatives are computed by taking the derivative of the basis functions $\mathbf{p}(x)$ in (2.2).

3. The RLW Equation and the FPM Numerical Implementation

In this section, we present RLW model, which is approximated by the FPM explained above. First, the partial differential equation (PDE) is presented by defining the appropriate initial and boundary conditions, and the relevant parameters needed to understand the behavior of the PDE are briefly discussed. Finally, we derive the discretized system by combining FD techniques for the time derivative and FPM for the spatial derivatives.

Let us consider the following form of the RLW equation:

$$u_t(x,t) + u_x(x,t) + \varepsilon \cdot u(x,t)u_x(x,t) - \mu \cdot u_{xxt}(x,t) = 0, \quad x \in \mathbb{R},\ t > 0, \tag{3.1}$$

with the physical conditions $u \to 0$ as $|x| \to \infty$. To the numerical implementation, we consider $a \le x \le b$ and the following boundary conditions:

$$u(a,t) = 0 \qquad u(b,t) = 0. \tag{3.2}$$

The initial condition for the problem (3.1) is given as follows:

$$u(x,0) = u_0(x), \quad a \le x \le b. \tag{3.3}$$

Parameters ε and μ in (3.1) are positive constants and are related by the *Stokes* number S defined as follows:

$$S = \frac{\varepsilon}{\mu}. \tag{3.4}$$

Usually, this number is set to 1 in order to balance the nonlinear effects of the advective and dispersive terms present in this problem.

In order to obtain the numerical approximation of (3.1), the time derivative of the RLW equation is calculated by applying a FD formula and the θ-weighted ($0 \le \theta \le 1$) scheme to the space derivative at two successive time levels n and $n+1$, where n is an integer that denotes the time step. The approximation is then given as follows:

$$\begin{aligned} &\frac{\widehat{u}^{n+1} - \widehat{u}^n}{\delta t} + \theta\left((\widehat{u}_x)^{n+1} + \varepsilon \cdot \widehat{u}^{n+1}(\widehat{u}_x)^{n+1}\right) + (1-\theta)\left((\widehat{u}_x)^n + \varepsilon \cdot \widehat{u}^n(\widehat{u}_x)^n\right) \\ &\quad - \frac{\mu}{\delta t}\left((\widehat{u}_{xx})^{n+1} - (\widehat{u}_{xx})^n\right) = 0, \end{aligned} \tag{3.5}$$

where $\widehat{u}^n = \widehat{u}(x,t^n)$, $t^n = t^{n-1} + \delta t$, and δt is the size of the time step. With the idea to adequately address the nonlinear term in (3.5), a linearized scheme given by the following expression is used [21, 46]:

$$\widehat{u}^{n+1}(\widehat{u}_x)^{n+1} \approx \widehat{u}^{n+1}(\widehat{u}_x)^n + \widehat{u}^n(\widehat{u}_x)^{n+1} - \widehat{u}^n(\widehat{u}_x)^n; \tag{3.6}$$

therefore, from (3.5) and (3.6), the following expression is obtained:

$$\begin{aligned}\widehat{u}^{n+1} + \delta t \cdot \theta\Big((\widehat{u}_x)^{n+1} + \varepsilon \cdot \Big[\widehat{u}^{n+1}(\widehat{u}_x)^n + \widehat{u}^n(\widehat{u}_x)^{n+1}\Big]\Big) - \mu \cdot (\widehat{u}_{xx})^{n+1} \\ = \widehat{u}^n + \delta t \cdot \big(\varepsilon \cdot (2\theta - 1)\widehat{u}^n(\widehat{u}_x)^n - (1-\theta)(\widehat{u}_x)^n\big) - \mu \cdot (\widehat{u}_{xx})^n.\end{aligned} \tag{3.7}$$

With the purpose to obtain the local approximation $\widehat{u}^{n+1}$, this work presents an alternative method based on the FPM, which was introduced in Section 2. Using (2.11) and (2.13), assume that $\theta = 1/2$ and replace into (3.7). Then the following discrete relation is obtained for the time level $n+1$:

$$\mathbf{G}_k \cdot \boldsymbol{\lambda}\left(\mathbf{X}^{\mathbf{k}}\right) = f_k, \tag{3.8}$$

where matrix $\mathbf{G}_k$ and the known quantity f_k (based on the time level n) are defined as follows:

$$\begin{aligned}\mathbf{G}_k &= \mathbf{N}^T + \frac{\delta t}{2} \cdot \mathbf{N_x}^T + \frac{\delta t}{2}\varepsilon \cdot \mathbf{N}^T \cdot \widehat{u}_x^n + \frac{\delta t}{2}\varepsilon \cdot \widehat{u}^n \cdot \mathbf{N}_x^T - \mu \cdot \mathbf{N}_{xx}^T, \\ f_k &= \widehat{u}^n - \frac{\delta t}{2} \cdot \widehat{u}_x^n - \mu \cdot \widehat{u}_{xx};\end{aligned} \tag{3.9}$$

here, the subscript k denotes the evaluation in the *star node* x_k.

Note that for simplicity, the terms $\mathbf{N}^T(x)$, $\mathbf{N}_x^T(x)$, and $\mathbf{N}_{xx}^T(x)$ have been replaced by $\mathbf{N}^T$, $\mathbf{N}_x^T$, and $\mathbf{N}_{xx}^T$, respectively. We remark that this shape functions are computed only at the beginning of calculation.

Otherwise, in the case of boundary points (see (3.2)), the matrix $\mathbf{G}_k$ and quantity f_k adopt the following forms, respectively:

$$\mathbf{G}_{a,b} = \mathbf{N}^T \qquad f_{a,b} = 0. \tag{3.10}$$

Finally, using (3.8) and (3.10) and taking into account the point collocation procedure for each of the N_p nodes that comprise the domain Ω, the following system of discrete equation is solved:

$$\mathbf{G} \cdot \boldsymbol{\lambda} = \mathbf{f}, \tag{3.11}$$

where $\mathbf{G}$ is defined as a stiffness matrix, $\boldsymbol{\lambda}$ represents the vector collecting of the point parameters λ^{n+1}, and $\mathbf{f}$ is a vector of known values brought from the time level n.

4. Test Problems

In this section, the results of the numerical solution of the RLW equation based on the FPM approach are presented. The numerical simulation includes the propagation of a solitary wave, the interaction of two positive solitary waves, the interaction of a positive and a negative solitary wave, the evaluation of *Maxwellian* pulse into stable solitary waves, and

Table 1: FPM parameters for the numerical simulation.

Total discretization points	N_p	300
Cloud size	N_c	5
Interpolation base function	m	4
Weighting function parameters	q and β	1 : 1 and 0 : 25

the development of an undular bore. According to [40], the RLW equation must comply with three conservation laws related to mass, momentum, and energy, which are given as follows:

$$\int_{-\infty}^{\infty} u\,\mathrm{d}x \approx C_1 = \int_a^b u\,\mathrm{d}x, \tag{4.1}$$

$$\int_{-\infty}^{\infty} \left(u^2 + \mu(u_{xx})^2\right)\mathrm{d}x \approx C_2 = \int_a^b \left(u^2 + \mu(u_{xx})^2\right)\mathrm{d}x, \tag{4.2}$$

$$\int_{-\infty}^{\infty} \left(u^3 + 3u^2\right)\mathrm{d}x \approx C_3 = \int_a^b \left(u^3 + 3u^2\right)\mathrm{d}x. \tag{4.3}$$

In the following test problems, the numerical solutions must control these conservation laws during propagation. Therefore, these quantities are used to measure the accuracy of the proposed method. All of the following test problems were developed using the FPM parameters shown in Table 1. It is worth mentioning that the following experiments have been extracted from previous works; see [10, 11, 19–21] for further details on the suitability of our proposal.

4.1. Propagation of a Single Solitary Wave

Solitary waves are wave packets or pulses that propagate nonlinearly in dispersive media. Due to the dynamic balance between the nonlinear and dispersive effects, these waves retain a stable waveform known as a soliton. This is a very special type of solitary wave, which also keeps its waveform after collision with other solitons [21]. In the case of solitons, the following explicit solution to (3.1) is given by [7]

$$u(x,t) = 3c\ \mathrm{sech}^2[k(x - x_0 - vt)], \tag{4.4}$$

which represents a single solitary wave of amplitude $3c$ centered at x_0 with velocity $v = 1+\varepsilon c$ and width $k = (1/2)\sqrt{\varepsilon c/\mu v}$. The initial condition of (3.1) is given as follows:

$$u(x,0) = 3c\ \mathrm{sech}^2[k(x - x_0)]. \tag{4.5}$$

The RLW parameters used in the numerical simulation are $c = 0.01, 0.055, 0.1$, $x_0 = 0$, $\varepsilon = \mu = 1 (S = 1)$ and $\delta t = 0.1$. As expected, the solitary wave moves to the right across

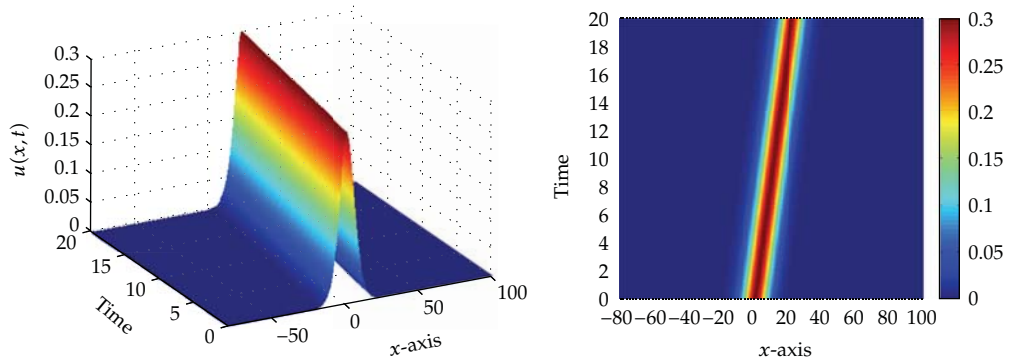

Figure 1: (a) Perspective and (b) superior view of the propagation of a single solitary wave for $c = 0.1$.

Table 2: Error norms and conservation quantities for the propagation of a single solitary wave for $c = 0.01$.

t	L_2	L_∞	C_1	C_2	C_3
0	0.000039	0.000041	1.205460	0.024167	0.072938
5	0.000060	0.000030	1.205479	0.024167	0.072938
10	0.000077	0.000030	1.205406	0.024167	0.072938
15	0.000083	0.000030	1.205303	0.024167	0.072938
20	0.000089	0.000043	1.205127	0.024167	0.072938

the space interval $-40 \leq x \leq 60$ in the time interval $0 \leq t \leq 20$. As in previous work, such as [20, 21], the boundary conditions are extracted from the exact solution (4.4), and the initial condition is given by (4.5). The FPM parameters are shown in Table 1. Moreover, based on the conservation laws Equations (3.9) and (3.10) and the explicit solution (4.4), the following error norms are calculated for this test problem:

$$L_2 = \sqrt{h\sum_{j=1}^{N_p}\left|u(x_j) - \widehat{u}(x_j)\right|^2},$$
$$L_\infty = \max_j\left|u(x_j) - \widehat{u}(x_j)\right|, \tag{4.6}$$

where h is the minimum distance between any two points in the domain $a \leq x \leq b$. The error norms L_2, L_∞ and conservation quantities C_1, C_2, and C_3 are shown in Tables 2, 3, and 4. A perspective and superior view of the propagation of a single solitary wave when $c = 0.1$ is shown in Figure 1. Moreover, Figure 2 presents the evolution of the L_2 and L_∞ error norms at different values of c.

The results obtained in this case show that the conservation quantities are controlled in different time steps, and moreover, the error norms L_2 and L_∞ are of the order of 10^{-4}, which demonstrate the remarkable accuracy of the proposed method and, therefore, the suitability of FPM for this kind of physical problem.

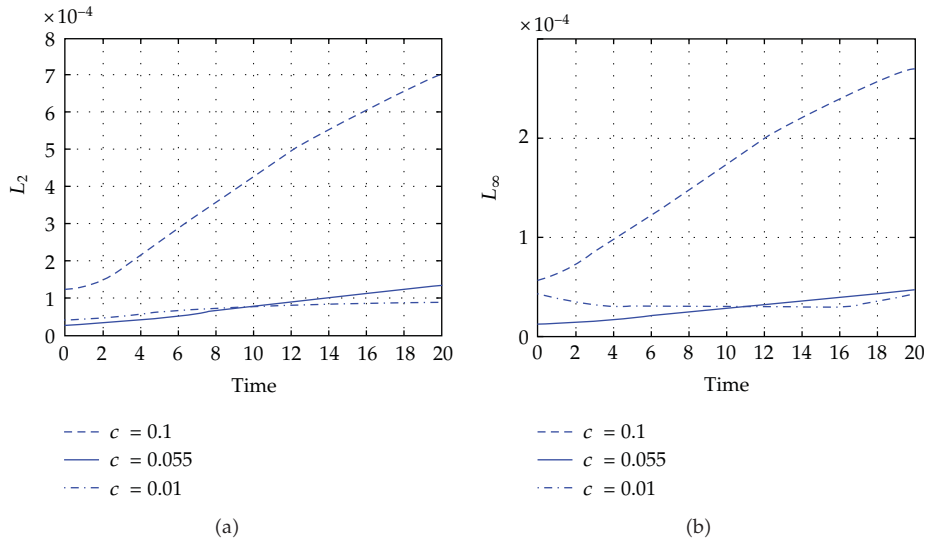

Figure 2: (a) L_2 and (b) L_∞ error norms for the propagation of a single solitary wave.

Table 3: Error norms and conservation quantities for the propagation of a single solitary wave for $c = 0.055$.

t	L_2	L_∞	C_1	C_2	C_3
0	0.000028	0.000012	2.890605	0.321290	0.995896
5	0.000045	0.000019	2.890605	0.321290	0.995896
10	0.000076	0.000028	2.890605	0.321290	0.995896
15	0.000106	0.000037	2.890605	0.321290	0.995896
20	0.000133	0.000047	2.890605	0.321290	0.995896

Table 4: Error norms and conservation quantities for the propagation of a single solitary wave for $c = 0.1$.

t	L_2	L_∞	C_1	C_2	C_3
0	0.000123	0.000058	3.979950	0.810520	2.579202
5	0.000249	0.000111	3.979950	0.810520	2.579202
10	0.000428	0.000172	3.979950	0.810521	2.579202
15	0.000580	0.000230	3.979950	0.810521	2.579202
20	0.000702	0.000268	3.979950	0.810521	2.579202

4.2. Interaction of Two Positive Solitary Waves

In this case, the numerical example consists on the interaction of two positive solitary waves defined by the following initial condition:

$$u(x,0) = \sum_{j=1}^{2} 3c_j \operatorname{sech}^2\left(k_j\left(x - x_j\right)\right), \tag{4.7}$$

Table 5: Conservation quantities for the interaction of two positive solitary waves.

t	C_1	C_2	C_3
0	37.916479	120.674902	745.391797
5	37.916674	120.676914	745.396694
10	37.916670	120.607313	744.749676
15	37.916673	120.409138	743.040480
20	37.916671	120.663186	745.265479
25	37.916672	120.678190	745.412442
30	37.916662	120.678701	745.417152

Table 6: Conservation quantities for the interaction of a positive and negative solitary wave.

t	C_1	C_2	C_3
0	−6.06072	383.42957	−354.233156
2	−6.06072	383.48023	−353.305989
5	−6.06072	406.31404	−379.084777
10	−6.06072	383.69552	−354.093811
15	−6.06072	383.64904	−353.883879
20	−6.07021	383.63883	−353.856241

with $c_j = 4k_j^2/(1 - 4k_j^2)$ and the boundary conditions:

$$u(a,t) = u(b,t) = 0. \tag{4.8}$$

The RLW parameters used in the numerical simulation are $k_1 = 0.4$, $k_2 = 0.3$, $x_1 = 15$, $x_2 = 35$, $\varepsilon = \mu = 1(S = 1)$, and $\delta t = 0.01$. This waves move across the space interval $0 \leq x \leq 120$ and the time interval $0 \leq t \leq 30$. Likewise, the FPM parameters used in this simulation are shown in Table 1. The results of the FPM approximation at different times are shown in Figures 3 and 4, where it is possible to observe that the higher amplitude solitary wave passes through the smaller wave with no change in its waveform. Once again, our results are in agreement with our expectations for all discrete time measured. As in the case of a solitary wave, the three quantities C_1, C_2, and C_3 are conserved see Table 5.

4.3. Interaction of a Positive and Negative Solitary Wave

This example focuses on the interaction of a positive and negative solitary wave, starting with the initial condition given by (4.7) and the boundary conditions defined in (4.8). The RLW parameters used in the numerical simulation are $k_1 = 0.4$, $k_2 = 0.6$, $x_1 = 23$, $x_2 = 38$, $\varepsilon = \mu = 1(S = 1)$, and $\delta t = 0.1$. The waves interact across the space interval $-10 \leq x \leq 80$ and the time interval $0 \leq t \leq 20$. As in the other cases, the FPM parameters are shown in Table 1. The results of the FPM approximation at different times are shown in Figures 5 and 6, where it is possible to observe that the collision produces additional solitary waves. Finally, note that the three conservation quantities for various times steps are controlled, as shown in Table 6.

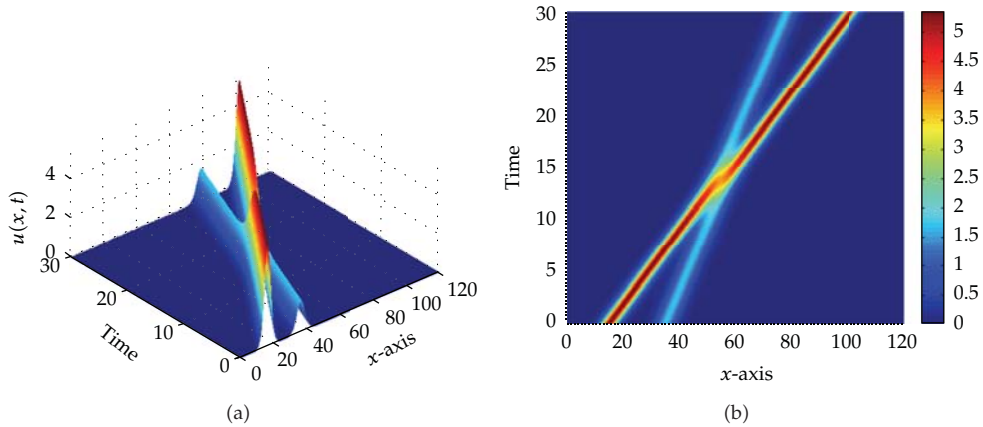

Figure 3: (a) Perspective and (b) superior view of the interaction of two positive solitary waves.

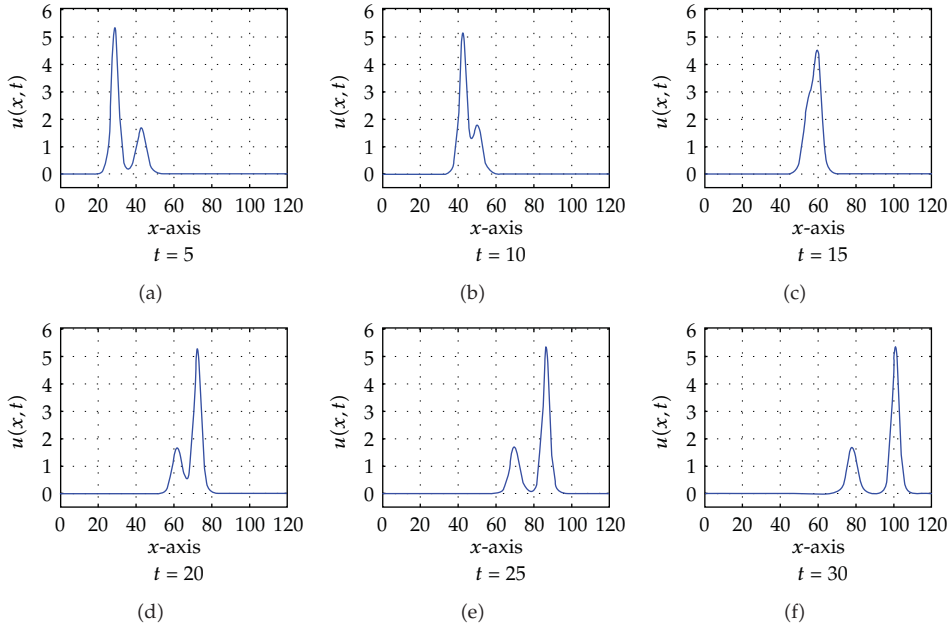

Figure 4: Detailed view of the interaction of two positive solitary waves at various times.

4.4. Evolution of Maxwellian Pulse into Stable Waves

This problem deals with the evolution of the *Maxwellian* pulse into stable solitary waves at various values of the parameter μ. The initial condition is given as follows:

$$u(x,0) = \exp\left[-(x-7)^2\right]. \tag{4.9}$$

The boundary conditions are defined as in (4.8). For this test, the RLW parameters for the numerical simulation are $\varepsilon = 1$, $\mu = 0.1$, 0.001, and 0.01, and $\delta t = 0.01$. This pulse is studied

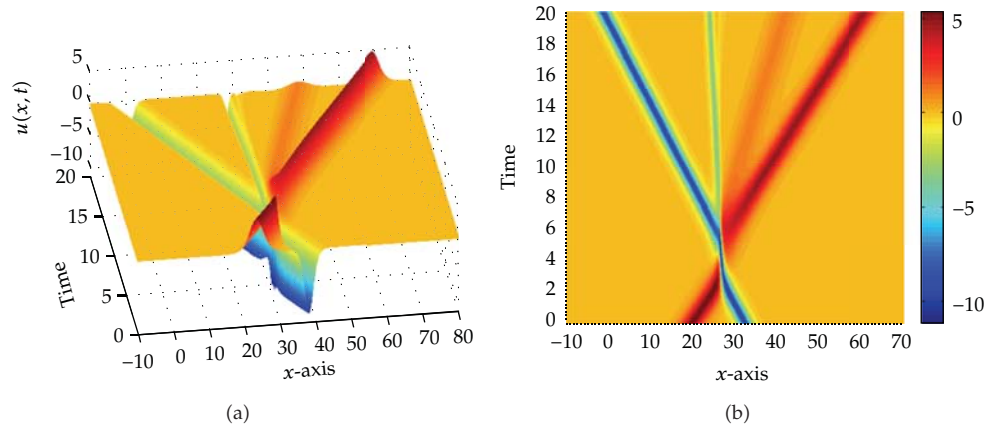

Figure 5: (a) Perspective and (b) superior view of the interaction of a positive and negative solitary wave.

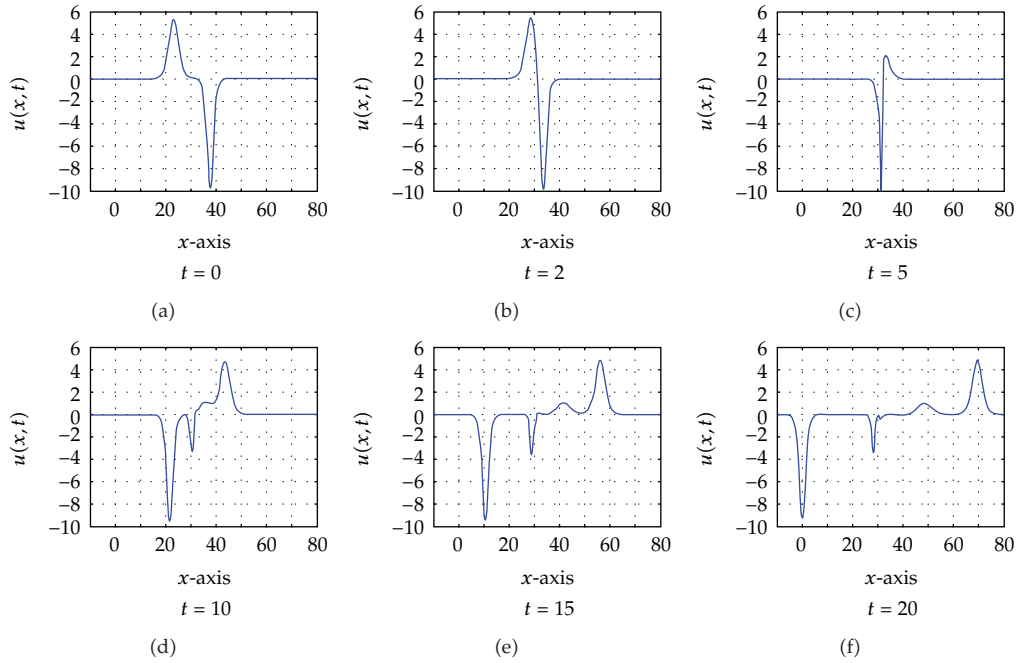

Figure 6: Detailed view of the interaction of a positive and negative solitary wave at various times.

across the space interval $0 \leq x \leq 30$ and time interval $0 \leq t \leq 10$ for the three cases of μ. The FPM parameters are shown in Table 1. The results of the FPM approximation at different values of the parameter μ are shown in Figures 7, 8, and 9, where it is possible to observe that the *Maxwellian* pulse develops into various solitary waves. As in the other experiments, the three conservation quantities for various times steps and values of parameter μ as given in Tables 7, 8, and 9 are controlled throughout the simulation.

Table 7: Conservation quantities for the evolution of the Maxwellian pulse into stable waves for $\mu = 0.1$.

t	C_1	C_2	C_3
0	1.772454	1.378633	4.783269
1	1.772454	1.378617	4.783257
2	1.772454	1.378531	4.783179
3	1.772454	1.378455	4.783110
4	1.772454	1.378412	4.783069
5	1.772454	1.378389	4.783043
6	1.772454	1.378375	4.783026
7	1.772454	1.378367	4.783015
8	1.772454	1.378361	4.783006
9	1.772454	1.378357	4.783000
10	1.772454	1.378354	4.782995

Table 8: Conservation quantities for the evolution of the Maxwellian pulse into stable waves for $\mu = 0.01$.

t	C_1	C_2	C_3
0	1.772454	1.265846	4.783269
1	1.772454	1.266067	4.784169
2	1.772454	1.267009	4.788193
3	1.772454	1.267889	4.792014
4	1.772454	1.268268	4.793725
5	1.772454	1.268398	4.794333
6	1.772454	1.268444	4.794551
7	1.772454	1.268463	4.794639
8	1.772454	1.268473	4.794680
9	1.772454	1.268479	4.794702
10	1.772454	1.268483	4.794716

Table 9: Conservation quantities for the evolution of the Maxwellian pulse into stable waves for $\mu = 0.001$.

t	C_1	C_2	C_3
0	1.772454	1.254567	4.783269
1	1.772454	1.254850	4.785121
2	1.772454	1.265146	4.859827
3	1.772454	1.274927	4.929081
4	1.772454	1.278024	4.950083
5	1.772454	1.278888	4.954447
6	1.772454	1.279216	4.955791
7	1.772454	1.279563	4.958827
8	1.772454	1.279775	4.960823
9	1.772454	1.279696	4.959418
10	1.772454	1.279591	4.957822

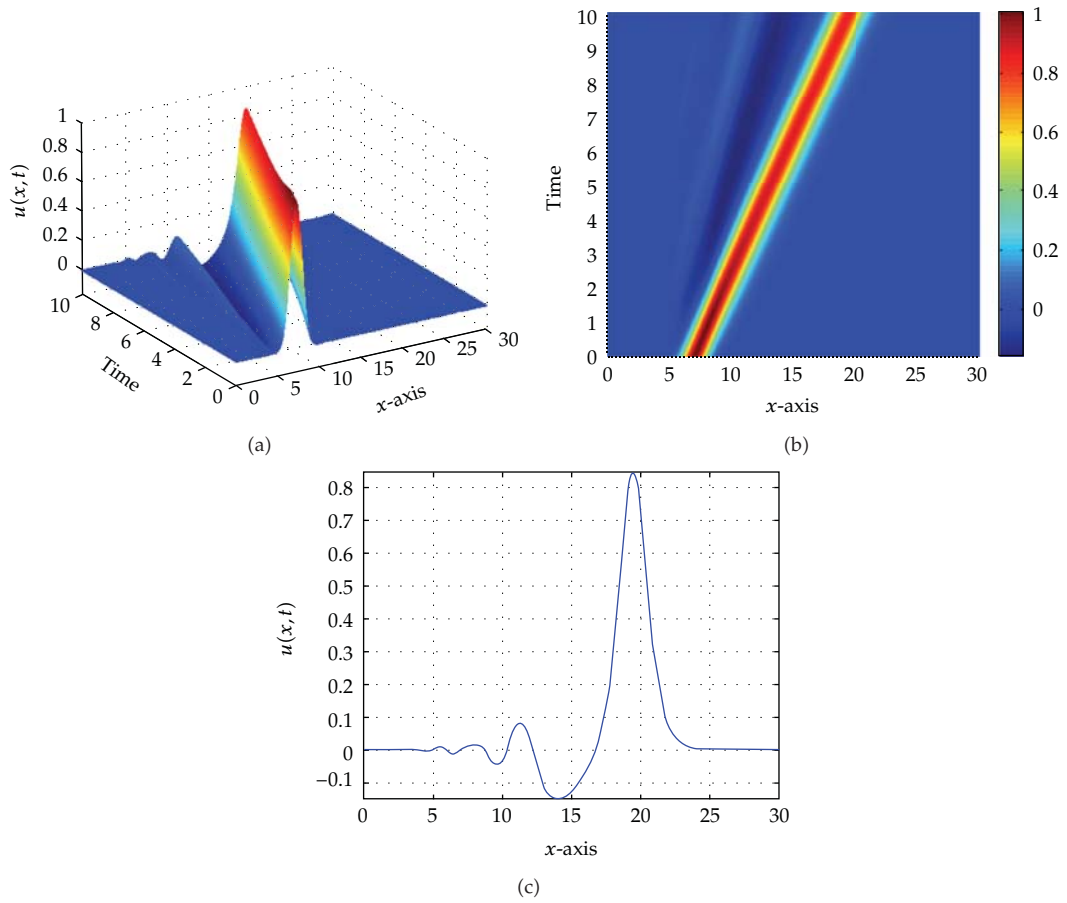

Figure 7: (a) Perspective, (b) superior, and (c) final detailed view of the evolution of the Maxwellian pulse into stable waves for $\mu = 0.1$.

4.5. Development of an Undular Bore

This numerical example allows us to study the development of an undular bore from the following initial condition:

$$u(x,0) = 0.5u_0\left[1 - \tanh\left(\frac{x - x_c}{d}\right)\right], \tag{4.10}$$

which represents the elevation of a water surface above equilibrium. The parameter u_0 is the change in water level at $x = x_c$, and d is the slope between still and deep water. Beside these conditions, the boundary conditions are defined by (4.8). The RLW parameters used for the numerical simulation are $\varepsilon = 3/2$, $\mu = 1/6$, and $\delta t = 0.1$. The undular bore is studied in the space interval $-36 \leq x \leq 300$ and time interval $0 \leq t \leq 250$. In addition, $u_0 = 0.1$, $x_c = 0$, and $d = 1, 2, 5$. The FPM parameters are shown in Table 1. An initial detailed view at different values of slope d is presented in Figure 10. The results of the FPM approximation at different

Table 10: Conservation quantities for the development of an undular bore for $d = 1$.

t	C_1	C_2	C_3
0	6.070750	0.602547	1.866131
50	11.438580	1.152584	3.571518
100	16.805366	1.701540	5.273289
150	22.184395	2.252770	6.982176
200	27.558493	2.802943	8.687707
250	32.933255	3.353220	10.393560

Table 11: Conservation quantities for the development of an undular bore for $d = 2$.

t	C_1	C_2	C_3
0	6.070750	0.597374	1.850512
50	11.435277	1.146559	3.553294
100	16.809517	1.696678	5.258797
150	22.185217	2.247110	6.965201
200	27.560092	2.797381	8.671063
250	32.935036	3.347666	10.376953

Table 12: Conservation quantities for the development of an undular bore for $d = 5$.

t	C_1	C_2	C_3
0	6.070750	0.582211	1.803261
50	11.435000	1.131142	3.505463
100	16.810000	1.681269	5.211217
150	22.185001	2.231499	6.917114
200	27.560001	2.781775	8.623046
250	32.935000	3.332064	10.328972

values of d are shown in Figures 11, 12, and 13, and the conservation quantities for various times steps are given in Tables 10, 11, and 12. In this particular problem, quantities C_1, C_2, and C_3 are not conserved but increase linearly according to the values of M_1, M_2, and M_3, respectively [47]:

$$\begin{aligned} M_1 &= \frac{\mathrm{d}}{\mathrm{d}t}C_1 = \frac{\mathrm{d}}{\mathrm{d}t}\int_{-\infty}^{\infty} u\,\mathrm{d}x = u_0 + \frac{1}{2}u_0^2, \\ M_2 &= \frac{\mathrm{d}}{\mathrm{d}t}C_2 = \frac{\mathrm{d}}{\mathrm{d}t}\int_{-\infty}^{\infty}\left(u^2 + \mu(u_x)^2\right)\mathrm{d}x = u_0^2 + \frac{2}{3}u_0^3, \\ M_3 &= \frac{\mathrm{d}}{\mathrm{d}t}C_3 = \frac{\mathrm{d}}{\mathrm{d}t}\int_{-\infty}^{\infty}\left(u^3 + 3u^2\right)\mathrm{d}x = 3u_0^2 + 3u_0^3 + \frac{3}{4}u_0^4. \end{aligned} \tag{4.11}$$

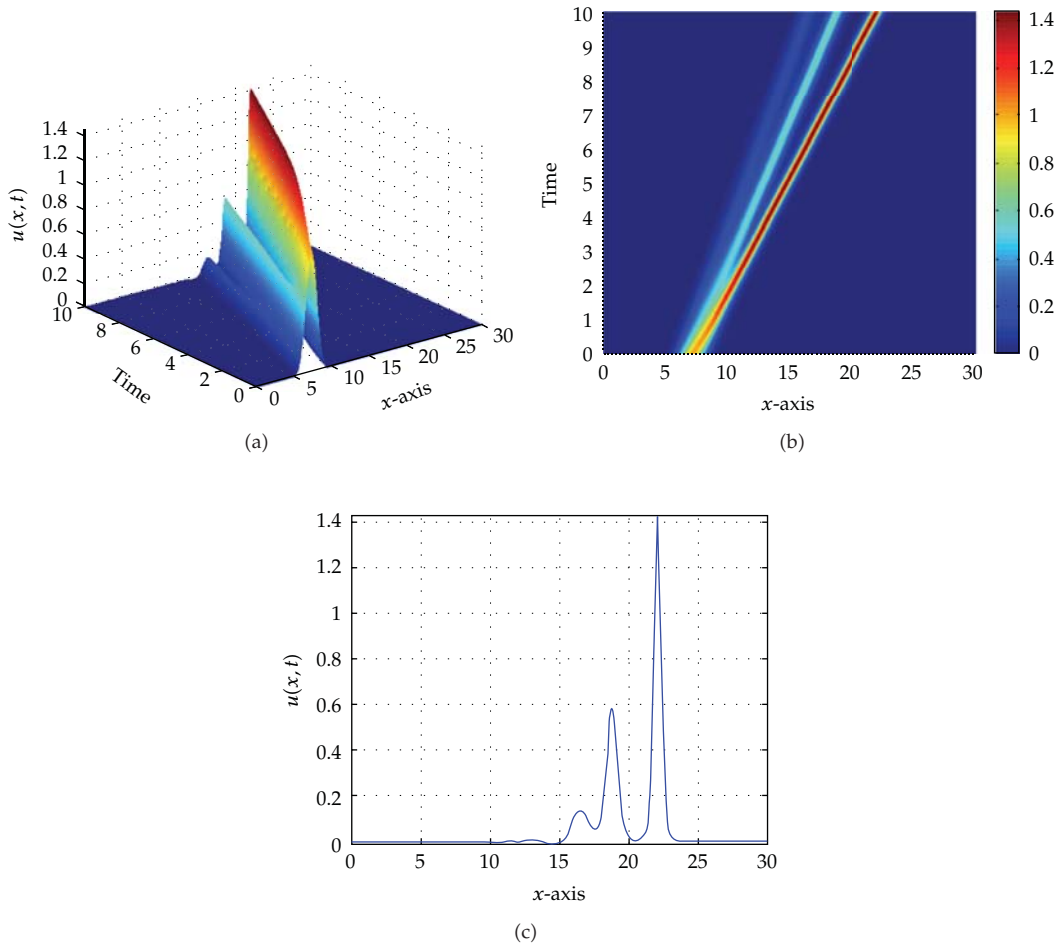

Figure 8: (a) Perspective, (b) superior, and (c) final detailed view of the evolution of the Maxwellian pulse into stable waves for $\mu = 0.01$.

Given the fixed value of u_0, the values of M_1, M_2, and M_3 are 0.105000, 0.010667 and 0.033075, respectively. With the values of M_1, M_2, and M_3 defined above and using $\Delta t = 50$, it is possible to calculate the increment in the quantities C_1, C_2, and C_3 as $\Delta C_1 = 5.25000$, $\Delta C_2 = 0.53335$ and $\Delta C_3 = 1.65375$, respectively. These increments are shown in Tables 10, 11, and 12 at different values of slope d.

5. Conclusions

The RLW equation is a PDE that can be used to solve several nonlinear physical problems. In fact, there exist various numerical approximations, such as FD, PS, and FEM, which are also suitable for this kind of problem.

In this paper, we present a meshless FPM as an alternative approach for the numerical solution of the RLW equation. About the FPM, we remark that the linearized algebraical

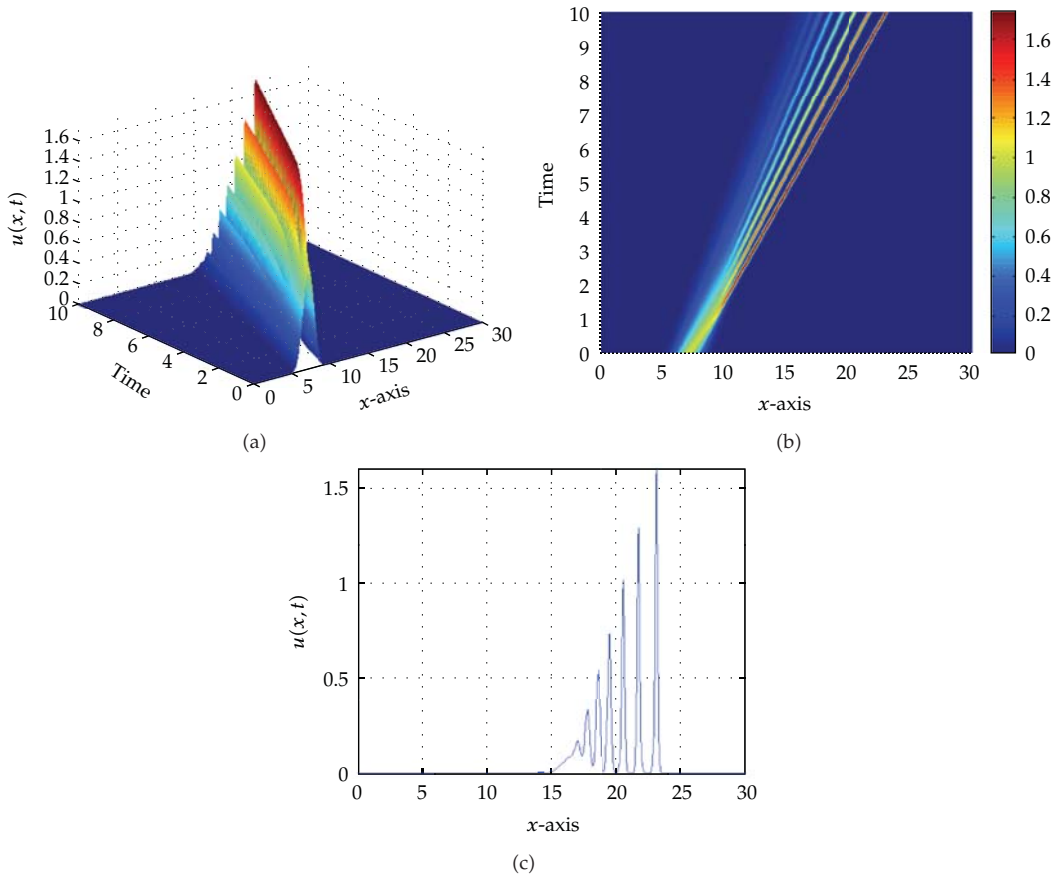

Figure 9: (a) Perspective, (b) superior, and (c) final detailed view of the evolution of the Maxwellian pulse into stable waves for $\mu = 0.001$.

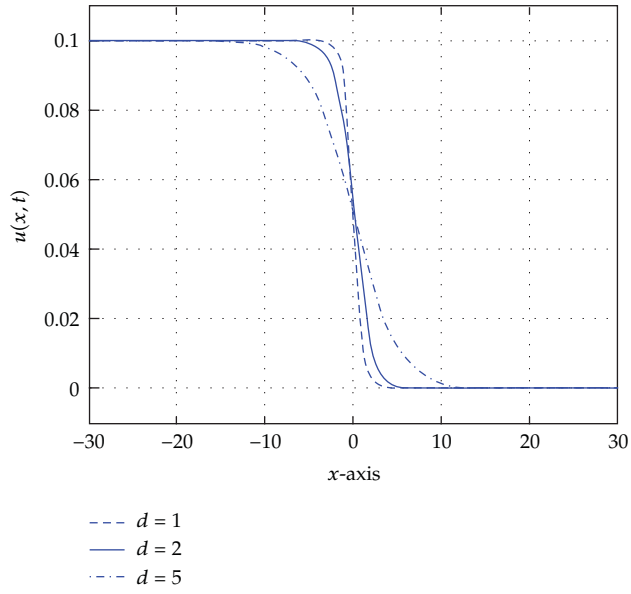

Figure 10: Initial detailed view of the development of an undular bore at different values of slope d.

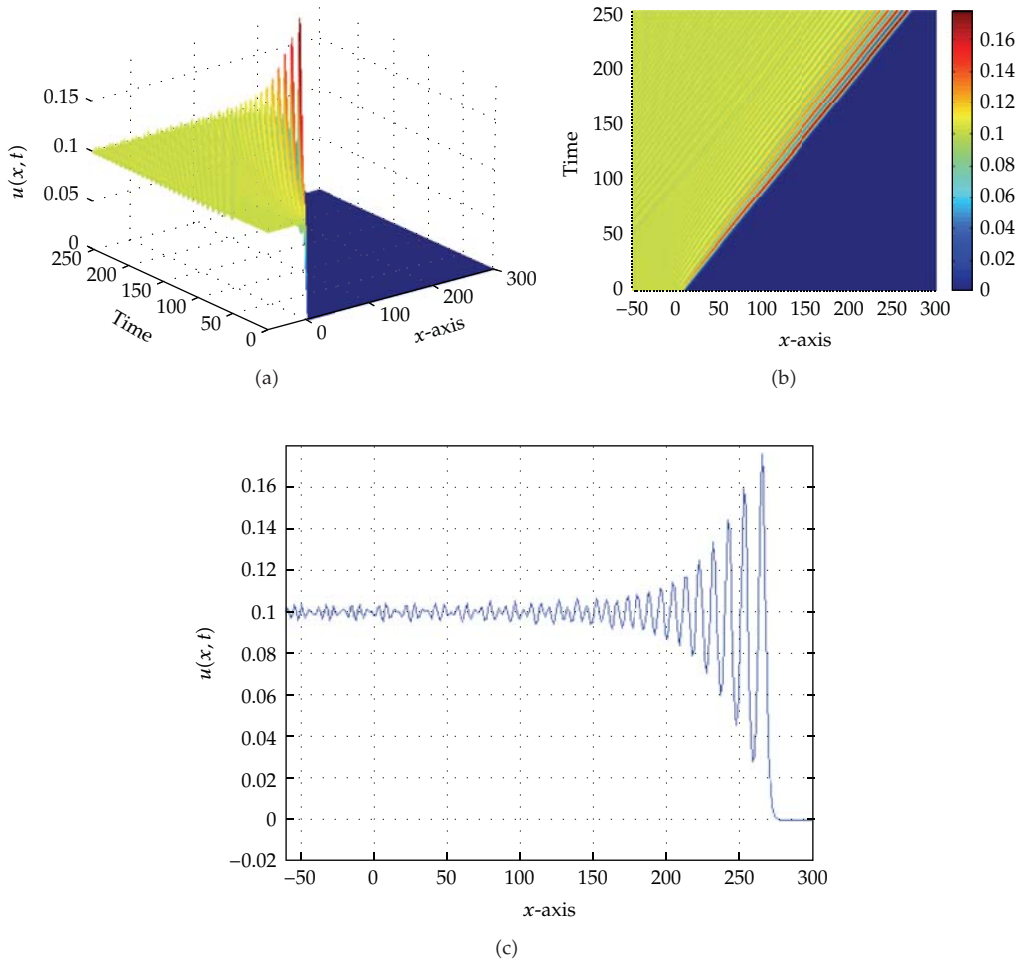

Figure 11: (a) Perspective, (b) superior, and (c) final detailed view of the development of an undular bore for $d = 1$.

system (3.8) is easy to implement, as shape functions are computed only at the beginning of calculation.

The efficiency of the proposed technique has been tested using different numerical experiments. The above is remarked by the comparision between exact and numerical solutions shown in Tables 2, 3, and 4 (see L_2, L_∞ error norms).

In cases in which precision (L_2, L_∞) cannot be evaluated, we verify the accuracy of the simulations by measuring the conservation quantities C_1, C_2 and C_3 at different time steps. Note that the values of C_1 are stables for different time step, as such quantity is defined in linear terms of u; see (4.3).

We have also presented relevant features of this equation in order to better understand the behavior of the model.

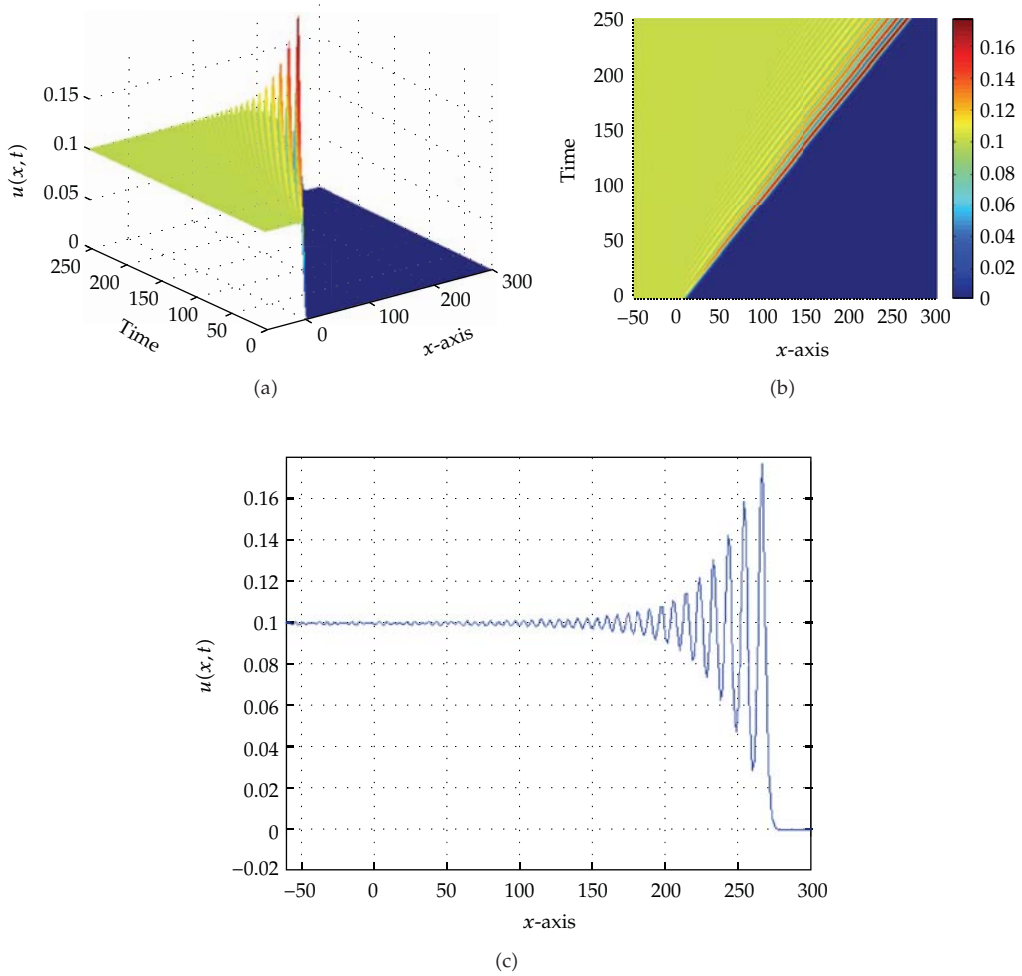

Figure 12: (a) Perspective, (b) superior, and (c) final detailed view of the development of an undular bore for $d = 2$.

The numerical test problems presented in Section 4 are in agreement with related literature; see [20, 21, 47].

According to the numerical results, we conclude that the present method can be considered a useful scheme for solving the type of nonlinear PDE considered here.

Acknowledgments

L. P. Pozo is partially supported by the Chilean Agency CONICYT (FONDECYT Project 11100253). C. Spa is partially supported by the Chilean Agency CONICYT (FONDECYT Project 3110046). The authors would also like to thank two anonymous reviewers for many helpful comments and suggestions on previous drafts of this paper.

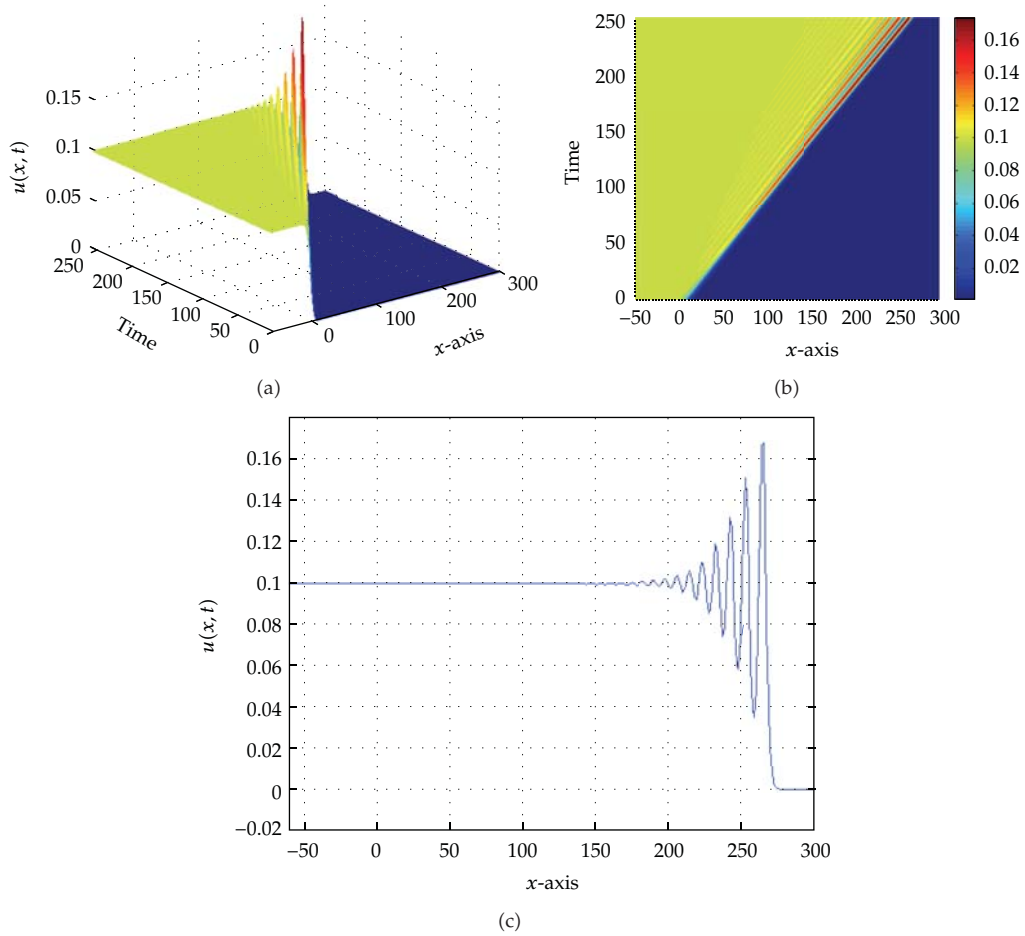

Figure 13: (a) Perspective, (b) superior, and (c) final detailed view of the development of an undular bore for $d = 5$.

References

[1] R. K. Dodd, J. C. Eilbeck, J. D. Gibbon, and H. C. Morris, *Solitons and Nonlinear Wave Equations*, Academic Press, London, UK, 1982.

[2] H. Washimi and T. Taniuti, "Propagation of ion-acoustic solitary waves of small amplitude," *Physical Review Letters*, vol. 17, no. 19, pp. 996–998, 1966.

[3] L. van Wijngaarden, "On the equation of motion for mixtures of liquid and gas bubbles," *The Journal of Fluid Mechanics*, vol. 33, pp. 465–474, 1968.

[4] D. Korteweg and F. de Vries, "On the change in form of long waves advancing in rectangular canal and on a new type of long stationary waves," *Philosophical Magazine*, vol. 39, pp. 422–443, 1895.

[5] J. Lin, Z. Xie, and J. Zhou, "High-order compact difference scheme for the regularized long wave equation," *Communications in Numerical Methods in Engineering with Biomedical Applications*, vol. 23, no. 2, pp. 135–156, 2007.

[6] B. Saka and I. Dag, "A numerical solution of the RLW equation by Galerkin method using quartic B-splines," *Communications in Numerical Methods in Engineering with Biomedical Applications*, vol. 24, no. 11, pp. 1339–1361, 2008.

[7] D. H. Peregrine, "Calculations of the development of an undular bore," *Journal of Fluid Mechanics*, vol. 25, pp. 321–330, 1966.

[8] J. L. Bona and P. J. Bryant, "A mathematical model for long waves generated by wavemakers in nonlinear dispersive systems," vol. 73, pp. 391–405, 1973.
[9] J. C. Eilbeck and G. R. McGuire, "Numerical study of the regularized long-wave equation. I. Numerical methods," *Journal of Computational Physics*, vol. 19, no. 1, pp. 43–57, 1975.
[10] D. Bhardwaj and R. Shankar, "A computational method for regularized long wave equation," *Computers & Mathematics with Applications. An International Journal*, vol. 40, no. 12, pp. 1397–1404, 2000.
[11] S. Kutluay and A. Esen, "A finite difference solution of the regularized long-wave equation," *Mathematical Problems in Engineering*, vol. 2006, pp. 1–14, 2006.
[12] B. Y. Guo and W. M. Cao, "The Fourier pseudospectral method with a restrain operator for the RLW equation," *Journal of Computational Physics*, vol. 74, no. 1, pp. 110–126, 1988.
[13] I. Dag, A. Dogan, and B. Saka, "B-spline collocation methods for numerical solutions of the RLW equation," *International Journal of Computer Mathematics*, vol. 80, no. 6, pp. 743–757, 2003.
[14] A. Esen and S. Kutluay, "Application of a lumped Galerkin method to the regularized long wave equation," *Applied Mathematics and Computation*, vol. 174, no. 2, pp. 833–845, 2006.
[15] I. Dag, B. Saka, and D. Irk, "Galerkin method for the numerical solution of the RLW equation using quintic B-splines," *Journal of Computational and Applied Mathematics*, vol. 190, no. 1-2, pp. 532–547, 2006.
[16] K. R. Raslan, "A computational method for the regularized long wave (RLW) equation," *Applied Mathematics and Computation*, vol. 167, no. 2, pp. 1101–1118, 2005.
[17] B. Saka, I. Da, and A. Dogan, "Galerkin method for the numerical solution of the RLW equation using quadratic B-splines," *International Journal of Computer Mathematics*, vol. 81, no. 6, pp. 727–739, 2004.
[18] B. Saka and I. Da, "A collocation method for the numerical solution of the RLW equation using cubic B-spline basis," *The Arabian Journal for Science and Engineering. Section A*, vol. 30, no. 1, pp. 39–50, 2005.
[19] R. Mokhtari and M. Mohammadi, "Numerical solution of GRLW equation using Sinc-collocation method," *Computer Physics Communications*, vol. 181, no. 7, pp. 1266–1274, 2010.
[20] A. Shokri and M. Dehghan, "A meshless method using the radial basis functions for numerical solution of the regularized long wave equation," *Numerical Methods for Partial Differential Equations*, vol. 26, no. 4, pp. 807–825, 2010.
[21] S.-U. Islam, S. Haq, and A. Ali, "A meshfree method for the numerical solution of the RLW equation," *Journal of Computational and Applied Mathematics*, vol. 223, no. 2, pp. 997–1012, 2009.
[22] T. Fries and H. Matthies, "Clasification and overview of meshfree methods," Informatikbericht-Nr, Technical University of Braunschweig, 2003.
[23] S. Li and W. K. Liu, *Meshfree Particle Methods*, Springer, Berlin, Germany, 2004.
[24] Y. Gu, "Meshfree methods and their comparisons," *International Journal of Computational Methods*, vol. 4, pp. 477–515, 2005.
[25] Y. Chen, J. Lee, and A. Eskandarian, *Meshless Methods in Solids Mechanics*, Springer, New York, NY, USA, 2006.
[26] V. P. Nguyen, T. Rabczuk, S. Bordas, and M. Duflot, "Meshless methods: a review and computer implementation aspects," *Mathematics and Computers in Simulation*, vol. 79, no. 3, pp. 763–813, 2008.
[27] E. Oñate, S. Idelsohn, O. C. Zienkiewicz, R. L. Taylor, and C. Sacco, "A stabilized finite point method for analysis of fluid mechanics problems," *Computer Methods in Applied Mechanics and Engineering*, vol. 139, no. 1Ó4, pp. 315–346, 1996.
[28] E. Oñate, S. Idelsohn, O. C. Zienkiewicz, and R. L. Taylor, "A finite point method in computational mechanics. Applications to convective transport and fluid flow," *International Journal for Numerical Methods in Engineering*, vol. 39, no. 22, pp. 3839–3866, 1996.
[29] E. Oñate and S. Idelsohn, "A mesh-free finite point method for advective-diffusive transport and fluid flow problems," *Computational Mechanics*, vol. 21, no. 4-5, pp. 283–292, 1998.
[30] E. Oñate, C. Sacco, and S. Idelsohn, "A finite point method for incompressible ow problems," *Computer Visual Science*, vol. 3, pp. 67–75, 2000.
[31] E. Oñate, F. Perazzo, and J. Miquel, "A finite point method for elasticity problems," *Computer and Structures*, vol. 49, pp. 2151–2163, 2001.
[32] F. Perazzo, S. Oller, J. Miquel, and E. Oñate, "Avances en el método de puntos finitos para la mecánica de sólidos," *Revista Internacional de Métodos Numéricos en Ingeniería*, vol. 22, pp. 153–168, 2006.
[33] F. Perazzo, J. Miquel, and E. Oñate, "A finite point method for solid dynamics problems," *Revista Internacional de Métodos Numéricos para Cálculo y Diseño en Ingeniería*, vol. 20, no. 3, pp. 235–246, 2004.
[34] L. Zhang, Y. Rong, H. Shen, and T. Huang, "Solidification modeling in continuous casting by finite point method," *Journal of Materials Processing Technology*, vol. 192-193, pp. 511–517, 2007.

[35] L. Pérez Pozo and F. Perazzo, "Non-linear material behaviour analysis using meshless finite point method," in *Proceedings of the 2nd Thematic Conference on Meshless Methods (ECCOMAS '07)*, pp. 251–268, 2007.

[36] L. Pérez Pozo, F. Perazzo, and A. Angulo, "A meshless FPM model for solving nonlinear material problems with proportional loading based on deformation theory," *Advances in Engineering Software*, vol. 40, no. 11, pp. 1148–1154, 2009.

[37] F. Perazzo, R. Lohner, and L. Pérez Pozo, "Adaptive methodology for meshless finite point method," *Advances in Engineering Software*, vol. 22, pp. 153–168, 2007.

[38] A. Angulo, L. Pérez Pozo, and F. Perazzo, "A posteriori error estimator and an adaptive technique in meshless finite points method," *Engineering Analysis with Boundary Elements*, vol. 33, no. 11, pp. 1322–1338, 2009.

[39] M. Bitaraf and S. Mohammadi, "Large de ection analysis of exible plates by the meshless finite point method," *Thin-Walled Structures*, vol. 48, pp. 200–214, 2010.

[40] P. J. Olver, "Euler operators and conservation laws of the BBM equation," *Mathematical Proceedings of the Cambridge Philosophical Society*, vol. 85, no. 1, pp. 143–160, 1979.

[41] P. S. Jensen, "Finite difference techniques for variable grids," *Computers and Structures*, vol. 2, no. 1-2, pp. 17–29, 1972.

[42] J. Peraire, J. Ppeiro, L. Formaggia, K. Morgan, and O. Zienkiewicz, "Finite element euler computations in three dimensions," *International Journal for Numerical Methods in Engineering*, vol. 26, no. 10, pp. 2135–2159, 1988.

[43] E. Ortega, E. Oñate, and S. Idelsohn, "An improved finite point method for tridimensional potential flows," *Computational Mechanics*, vol. 40, no. 6, pp. 949–963, 2007.

[44] F. Perazzo, *Una metodología numérica sin malla para la resolución de las ecuaciones de elasticidad mediante el método de puntos finitos*, Doctoral thesis, Universitat Politécnica de Cataluña, Barcelona España, 2002.

[45] R. Taylor, S. Idelsohn, O. Zienkiewicz, and E. Oñate, "Moving least square approximations for solution of differential equations," CIMNE Research Report 74, 1995.

[46] S. G. Rubin and R. A. Graves Jr., "A cubic spline approximation for problems in fluid mechanics," NASA STI/Recon Technical Report 75, 1975.

[47] S. I. Zaki, "Solitary waves of the splitted RLW equation," *Computer Physics Communications*, vol. 138, no. 1, pp. 80–91, 2001.

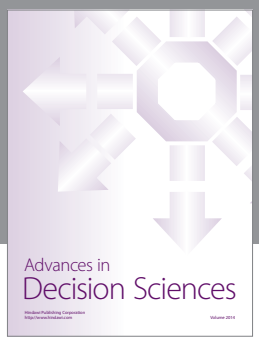

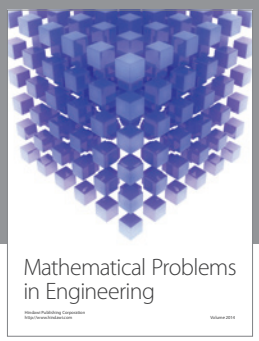

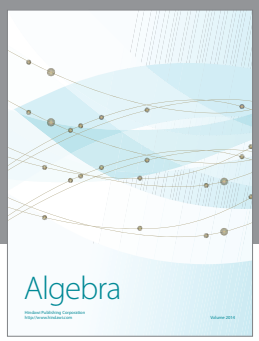

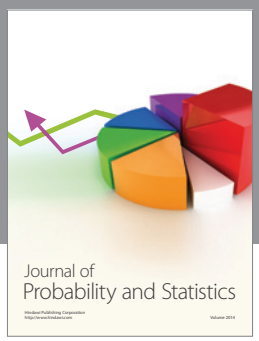

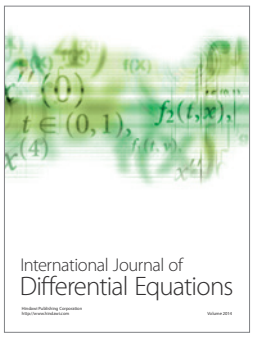

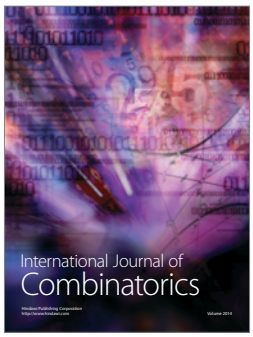

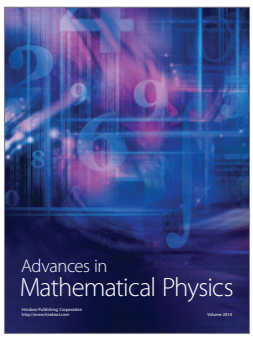

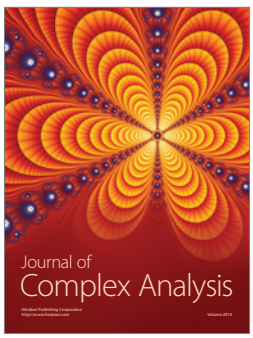

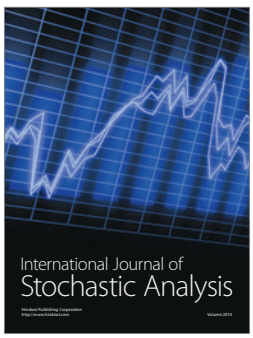

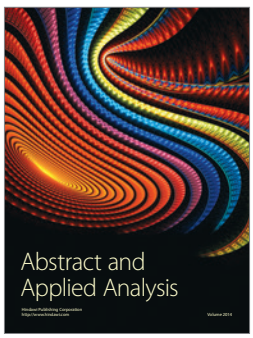

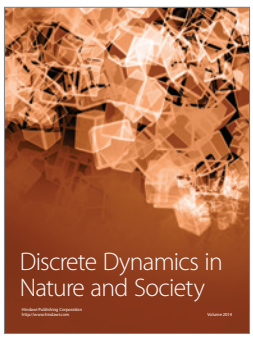

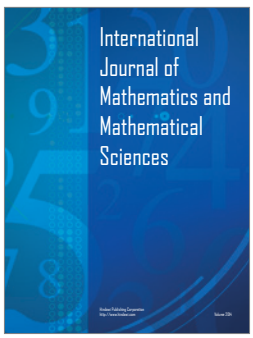

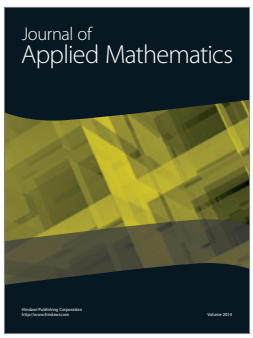

Hindawi
Submit your manuscripts at
http://www.hindawi.com